RSC Advances

PAPER

View Article Online
View Journal | View Issue

Cite this: *RSC Adv.*, 2024, **14**, 28791

Novel halogenated cyclopentadienyl hafnium precursor for atomic layer deposition of high-performance HfO_2 thin film†

Sangwook Park,‡[a] Yoona Choi,‡[b] Sunwoo Park,[a] Hayoon Lee,[a] Kiho Lee,[a] Jongwook Park *[a] and Woojin Jeon *[b]

High dielectric constant (high-*k*) materials play a crucial role in modern electronics, particularly in semiconductor applications such as transistor gate insulators and dielectrics in metal–insulator–metal (MIM) capacitors. However, achieving optimal crystallinity and suppressing interfacial layer formation during deposition processes remain key challenges. To address these challenges, this study introduces a novel approach using atomic layer deposition (ALD) with a new Hf precursor incorporating an iodo ligand. The synthesized precursor, IHf, demonstrates enhanced thermal stability and reactivity, leading to superior film properties. ALD deposition of HfO_2 thin films using IHf yields excellent crystallinity and effectively inhibits interfacial layer formation, resulting in enhanced capacitance density and improved leakage current characteristics in MIM capacitors. Notably, IHf-deposited HfO_2 films exhibit a significant reduction in leakage current, achieving an equivalent oxide thickness of 1.73 nm at a leakage current density of 7.02×10^{-8} A cm^{-2} @ +0.8 V. These findings highlight the potential of IHf as a promising precursor for high-performance electronic device fabrication, paving the way for advancements in semiconductor technology.

Received 12th August 2024
Accepted 4th September 2024

DOI: 10.1039/d4ra05848h

rsc.li/rsc-advances

Introduction

High dielectric constant (high-*k*) materials have various applications in electronics. Among them, the most state-of-the-art application is in the semiconductor field, particularly in areas such as the gate insulator of transistors and dielectrics in metal–insulator–metal (MIM) capacitors.[1–3] The high-*k* properties and insulation characteristics greatly influence the performance of these components. In the semiconductor field, high-*k* materials are formed through bottom-up processes *via* deposition techniques, and the physical thickness is reduced due to advancements in device integration and scaling.[4] Therefore, there is a need for deposition processes that utilize atomic layer deposition (ALD) to achieve excellent crystallinity and suppress substrate and interface layer formation.[5–7]

In particular, in ALD processes, it is necessary to form crystallization seeds during the deposition stage to achieve the desired crystal structure and crystallinity.[8–10] One method to enhance both the crystal structure and crystallinity of high-*k* thin films is by increasing the deposition temperature.[11] However, there is a limitation on raising the deposition temperature due to the thermal decomposition of precursors in ALD processes[12–14]. To overcome this issue, the Chung research group introduced *N*-alkoxy carboxamidate ligands into the precursors. The incorporation of these ligands improved the volatility and thermal characteristics of the precursor, resulting in enhanced high-temperature reactivity.[15] Particularly, derivatives such as $HfCp(edpa)_3$, composed of a cyclopentadienyl ligand and three carboxamidate ligands, demonstrated high thermal stability and rapid crystallization. However, these compounds suffer from increased viscosity and a melting point range of 62–135 °C, which renders them solid at room temperature, thus posing drawbacks for ALD processes. Therefore, this study proposes new derivatives that can enhance the thermal stability of ALD precursors.

In this study, we present an ALD process for HfO_2 using a novel Hf precursor with an iodo ligand. By introducing the iodo ligand, which exhibits relatively low reactivity compared to other halide precursors,[16–19] we synthesized a new precursor, IHf, which offers increased thermal stability and higher chemical adsorption density compared to conventional halide precursors. The ALD process using IHf and O_3 yielded HfO_2 thin films with excellent crystallinity and effectively suppressed the formation of interfacial layers when used with TiN as bottom

[a]*Integrated Engineering, Department of Chemical Engineering, Kyung Hee University, Deogyeong-daero, Giheung-gu, Yongin-si, Gyeonggi-do 17104, Republic of Korea. E-mail: jongpark@khu.ac.kr*

[b]*Department of Advanced Materials Engineering for Information and Electronics, Integrated Education Program for Frontier Science & Technology (BK21 Four), Kyung Hee University, Deogyeong-daero, Giheung-gu, Yongin-si, Gyeonggi-do 17104, Republic of Korea. E-mail: woojin.jeon@khu.ac.kr*

† Electronic supplementary information (ESI) available. See DOI: https://doi.org/10.1039/d4ra05848h

‡ Sangwook Park and Yoona Choi contributed equally to this work as first authors.

electrode material. This resulted in an increase in capacitance density in the TiN/HfO_2/TiN MIM capacitor due to the increased dielectric constant of HfO_2 and simultaneous improvement in leakage current characteristics by inhibiting interfacial layer formation. Particularly noteworthy is the significant improvement in leakage current characteristics, achieving an equivalent oxide thickness of 1.73 nm at a leakage current density of 7.02×10^{-8} A cm^{-2} @ +0.8 V in the HfO_2 single layer.

Results and discussion

Molecular design concept and synthesis

In this study, CpHf, which is currently commercialized in the industry, was used as reference materials for comparing the results and characteristics of the synthesized compounds.[20–22] Herein, we synthesized a novel precursor compound including an iodine atom on the cyclopentadienyl group to introduce an inductive effect and thereby strengthen the bonding strength with the central metal. Scheme 1 illustrates the chemical structure of the synthesized compound. IHf is an organometallic compound, where the cyclopentadienyl group having a halide substituent and dimethylamine ligands interact with the transition metal Hf.

The newly synthesized compound was obtained through a three-step synthesis process (Scheme 2). The starting material, cyclopentadiene, was synthesized *via* retro-Diels–Alder reaction and cracking distillation of dicyclopentadiene, achieving a yield of 91% without additional purification. The obtained cyclopentadiene was then subjected to substitution with lithium using *n*-BuLi reagent. Confirmation of lithium substitution was achieved using ^{1}H-NMR spectroscopy. As the reaction progressed, multiplet peaks at δ 6.61 and δ 6.49, as well as the pentet peak at δ 3.01 representing cyclopentadiene, disappeared, while a new singlet peak emerged at δ 5.32, indicating successful lithium substitution. In the second step, upon introducing iodine, the appearance of a singlet peak at δ 5.04 and doublet peaks at δ 5.96 and δ 6.10 confirmed the formation of the desired product. In the final synthesis step, the resulting product was confirmed through ^{1}H-NMR spectroscopy. The final synthesized compound exhibited a proton singlet peak around δ 2.84 representing dimethylamine and a proton triplet peaks at δ 5.74, 6.04 attributed to iodocyclopentadiene (Fig. S1†). The purity of the IHf precursor is over 98%, and the content of metals has been confirmed to be below 1 ppb for all 12 types of metals. The 12 types of metals are Ag, Au, Cd, Co, Li, Mg, Mn, Ni, Pb, Sn, V, and W atoms. As shown in Scheme 2 and Fig. S2,† the purity of the ligand compound (2) was confirmed to be over 99% through high-performance liquid chromatography (HPLC) experiments. Therefore, it can be confirmed that there is no CpHf content in the final compound, IHf precursor.

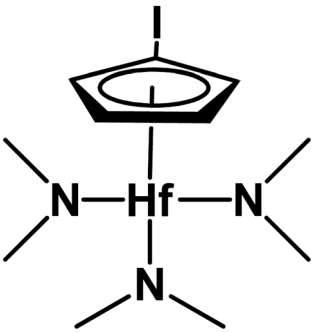

IHf

Scheme 1 Chemical structure of the synthesized compound.

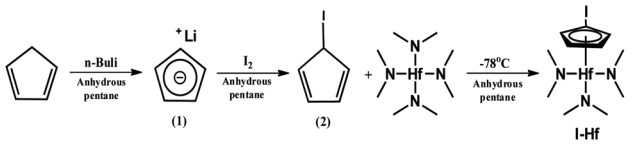

Scheme 2 Synthetic routes of the synthesized material.

Growth and characterization of high-*k* films

We evaluated the deposition behavior of HfO_2 by ALD using an IHf precursor. First, the thermal decomposition characteristics of the precursors were examined (Fig. 1(a)). The extent of precursor decomposition was measured at each temperature by injecting only the precursor without any reactants ((precursor feeding for 5 s − precursor purge for 20 s) × 50 cy). Both CpHf and IHf exhibited negligible thermal decomposition at 300 °C, with deposition rates of 0.001 nm s^{-1}. For CpHf, thermal decomposition began at 325 °C, reaching rates of 0.0024 and 0.0049 nm s^{-1} at 340 and 370 °C, respectively. In contrast, IHf showed a slight increase to 0.0018 nm s^{-1} at 340 °C, with a low

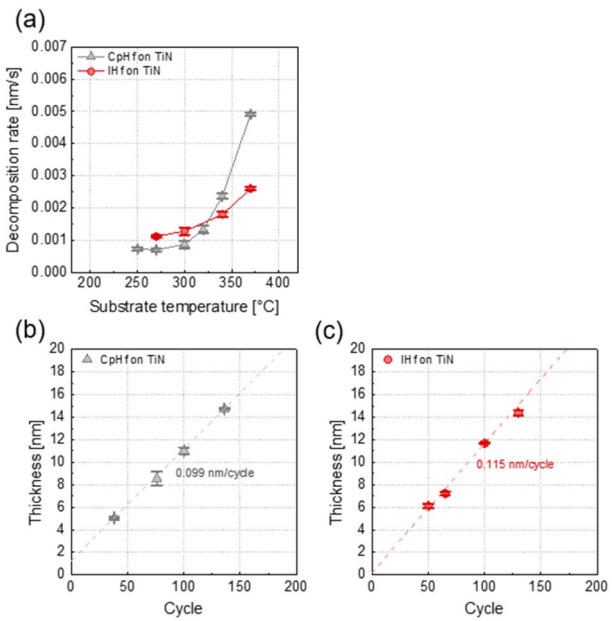

Fig. 1 (a) Thermal decomposition of CpHf and IHf precursors. Linear growth behavior of HfO_2 thin film deposition processes using (b) CpHf + O_3 and (c) IHf + O_3.

thermal decomposition rate of 0.0026 nm s^{-1} even at 370 °C. This indicated the enhanced high-temperature stability of IHf compared to CpHf. ALD deposition behavior using ozone as co-reactant at 300 °C was evaluated (Fig. 1(b)), within the ALD temperature window of both precursors, showing that HfO_2 deposition rate is slightly larger with IHf (0.115 nm per cycle) compared to CpHf (0.099 nm per cycle), indicating a higher saturation adsorption density on the TiN surface. According to XRR analysis (Fig. S3†), the density of HfO_2 deposited using CpHf was 7.75 g cm^{-3}, while the density of HfO_2 deposited using IHf was 8.91 g cm^{-3}. This indicates that HfO_2 films deposited with IHf are denser. These results are related to the chemisorption behavior differences between CpHf and IHf. Similar to CpHf, IHf chemically adsorbs in the gas phase during precursor supply, leading to the dissociation of the $-NMe_2$ ligand from the central metal.[23] The bond dissociation energy values for this process were calculated through molecular simulations and summarized in Table S1.† The bond dissociation energy is 851.111 kJ mol^{-1} for CpHf, whereas for IHf, it is 862.117 kJ mol^{-1}, indicating an increase of 11.006 kJ mol^{-1} in the energy required for $-NMe_2$ ligand dissociation.

The surface morphology and crystallinity difference of HfO_2 films deposited using CpHf and IHf precursors was analyzed (Fig. 2). O_3 was used as the reactant, and deposition temperature was kept constant at 300 °C. HfO_2 thin films deposited using CpHf and IHf do not exhibited any significant difference in morphology, as shown in AFM analyses (Fig. S4†). As-deposited films with CpHf showed no distinct crystallization peak up to a thickness of 15 nm, indicating an amorphous state. However, after post-deposition rapid thermal annealing (PDA) at 600 °C for 30 s under a N_2 atmosphere, crystallization-induced diffraction peaks were observed, showing a mixture of monoclinic and tetragonal phases. Notably, distinct peaks were only evident at a thickness of 15 nm, diminishing as the film thickness decreased to 10 and 7 nm, resembling the amorphous state. Conversely, films deposited with IHf exhibited broad peaks around 30–35°, indicating a meso-crystalline structure instead of amorphous, even in the as-deposited state.[24] This suggests that crystalline seeds were embedded with IHf deposition at 300 °C, leading to significantly higher crystallinity after annealing. XRD results of HfO_2 thin films after conducting PDA revealed much stronger and clearer diffraction peaks for IHf-deposited films compared to CpHf, even at 7 nm thickness, indicating more effective induction of crystallization by IHf precursors from the as-deposited state and enhanced crystallinity after annealing.

The chemical state analysis of the deposited HfO_2 films was confirmed using XPS (Fig. 3). The oxidation state of Hf was analyzed using Hf 4f spectra, showing no significant difference between films deposited with CpHf and IHf, both confirming Hf^{4+} oxidation states. However, depth profiling revealed differences between the precursors. In the HfO_2 film deposited using CpHf, approximately 3 at% of nitrogen content was shown (Fig. 3(b)). Furthermore, nitrogen content was not detected on the surface of the film, but it was observed after 4 seconds of Ar sputtering. Particularly, on the nitrogen-free surface of the HfO_2 film, the Hf : O ratio was 36.4 : 63.6 at%, indicating a favorable O/Hf ratio of 1.75. However, in the film where nitrogen content was detected, the film exhibited an O/Hf ratio of 40.3 : 56.5 at%, resulting in an O/Hf ratio of 1.40, indicating a highly oxygen-deficient composition. In contrast, in the HfO_2 film deposited with IHf, no nitrogen content was detected, and the Hf : O ratio was 34.5 : 65.4 at%, indicating an ideal stoichiometry with an O/Hf ratio of 1.89 (Fig. 3(c)). To identify the cause of nitrogen content in HfO_2 films deposited with CpHf, N 1s spectra were analyzed. In HfO_2 films deposited with CpHf, the oxidation state of nitrogen included in the film was confirmed at etch times of 15 s and 50 s, revealing oxidized TiN (Ti–O–N) states with a binding energy of 398.4 eV at both locations.[25,26] Conversely, the oxidation state of nitrogen in HfO_2 films deposited with IHf showed Ti–N bonding with a binding energy of 397.7 eV.[27,28] This indicates that the TiN bottom electrode undergoes oxidation damage by O_3 when deposited with CpHf. This is related to the difference in deposition rates observed in Fig. 1. In ALD, the deposition rate is determined by the chemisorption density of precursors, which is reduced by the steric hindrance effect, where the adsorption sites are blocked by the physical size of the ligands, and the screening effect, where the adsorption sites are blocked by physisorption of precursors.[29–31]

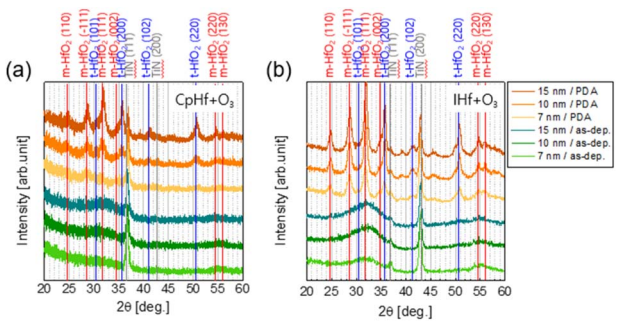

Fig. 2 XRD patterns of HfO_2 thin films deposited on 300 °C using (a) CpHf + O_3, and (b) IHf + O_3.

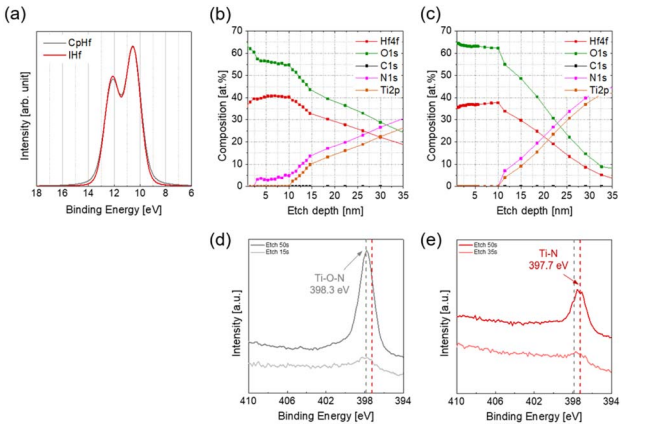

Fig. 3 (a) Hf 4f spectra of 10 nm-thick HfO_2 thin films deposited using CpHf and IHf precursors. (b and c) Depth profile of 10 nm-thick HfO_2 thin films deposited using (b) CpHf, and (c) IHf. (d and e) N 1s spectra obtained at each etch time from HfO_2 thin films deposited using (d) CpHf, and (e) IHf.

Surfaces that are not covered by adsorbates due to these effects are subsequently exposed to the reactant during the reactant feeding step. Particularly, on substrates with high reactivity with oxygen such as TiN, surface oxidation occurs, leading to the formation of interfacial layers. Thus, the lower deposition rate with CpHf indicates that more TiN substrate exposure occurs due to these effects compared to IHf, resulting in more severe oxidation damage of the TiN substrate, appearing as Ti–O–N. TEM analyses were conducted to investigate the formation of the interfacial layer based on the precursors (Fig. S5†).[32] In the case of CpHf, a relatively significant interfacial layer (IL) formation is observed, which corresponds well with the XPS results. Especially, Ti O–N formed by TiN oxidation damage is in an unstable state, leading to additional oxidation to TiO_2 and causing an oxygen scavenging effect, which assumes additional oxygen from the deposited metal oxide film.[30] Moreover, this additional oxidation may also induce some N diffusion from the TiN substrate into the HfO_2 thin film, as evidenced from the relatively high N-contamination level within the depth of the HfO_2 thin film (Fig. 3(b)). Therefore, it can be inferred that the formation of Ti–O–N interfacial layers contributes to the low O/Hf ratio and to N incorporation in HfO_2 films deposited with CpHf. This TiON interface formation with CpHf precursor can be further accounted for in Fig. 1(b), with the larger increase in thickness with CpHf as compared to IHf at temperatures larger than 325 °C. Consequently, IHf can be considered a more effective Hf precursor than CpHf for ALD deposition of HfO_2 films, as it suppresses TiN substrate oxidation damage, thereby inhibiting interfacial layer formation ensuring improved O/Hf stoichiometry and preventing N contamination in HfO_2 thin films. Consequently, IHf can be considered a more effective Hf precursor than CpHf for ALD deposition of HfO_2 films, as it suppresses TiN substrate oxidation damage, thereby inhibiting interfacial layer formation and ensuring O/Hf stoichiometry.

This improved suppression of interfacial layer formation also affects the enhanced crystallinity observed in Fig. 2. Unlike CpHf, which is hindered in crystallization by nitrogen content and oxygen deficiency, IHf forms crystalline seeds from the as-deposited state due to fewer impurities and ideal O/Hf stoichiometry. Additionally, crystallization due to the template effect of cubic TiN likely contributes to the high crystallinity of HfO_2 films deposited with IHf.

These results enable potential improvements in the characteristics of HfO_2 films deposited by ALD using IHf precursors. The thermal stability of each precursor is influenced by the cyclopentadienyl ligand binding to the central metal during chemical adsorption. Hence, the enhanced thermal stability of IHf is attributed to the incorporation of the halide group iodine in the cyclopentadienyl ligand. This can be explained by the molecular weight effect due to the introduction of iodine. The molecular weight of IHf is 501.71 g mol^{-1}, which is increased by 125.91 g mol^{-1} compared to CpHf. As a result of this increase in molecular weight, organometallic compounds achieve relatively higher thermal stability while maintaining their liquid form and electronic state.[33,34] Despite these results, IHf demonstrates superior reactivity compared to traditional precursors, where increased thermal stability often leads to decreased reactivity. These results suggest that the addition of the iodine halide group induces an electron-withdrawing effect through the cyclopentadienyl group, relatively reducing the electron density around the hafnium central metal. Consequently, the bond dissociation energy between the dimethylamine group and the hafnium central metal increases. As a result, due to the strong bond energy, IHf material gains the advantage of being capable of deposition even at relatively higher temperatures.

These improvements in crystallinity and suppression of interfacial layer formation led to enhanced electrical properties in metal–insulator–metal (MIM) capacitors of TiN/HfO_2/TiN structure (Fig. 4). Firstly, the bulk dielectric constants were determined *via* a physical thickness *versus* equivalent oxide thickness (t_{phy}–t_{ox}) plot (Fig. 4(a)). The inverse of the slope of (t_{phy}–t_{ox}) plot can be used to determine the bulk dielectric constant. The bulk dielectric constants of the HfO_2 films deposited with CpHf and IHf were measured to be 12.8 and 16.9, respectively. Dielectric constants below 20 are attributed to crystallization into the monoclinic phase. And, relatively higher crystallinity of HfO_2 thin film deposited using IHf attributed to relatively higher dielectric constant than that of CpHf.[7] Next, the leakage current characteristics of the MIM capacitors were examined through leakage current density *versus* applied voltage (J–V) curves. The J value of HfO_2 films deposited with IHf was 2–3 orders of magnitude lower than that of the films deposited with CpHf in all examined thicknesses. This improvement can be attributed to enhancements in the intrinsic properties of HfO_2 and improvements in the interfacial layer with TiN. Firstly, degradation in leakage current characteristics due to intrinsic aspects related to nitrogen content within the HfO_2 films deposited with CpHf is identified. Additionally, relatively oxygen deficient composition in the CpHf-deposited films would cause severe leakage current. The main carrier conduction in HfO_2 occurs through Poole–Frenkel (P–F) emission, which involves the detrap of electrons trapped at defect sites within the HfO_2 film.[35,36] The defects contributing to P–F emission are primarily associated with oxygen vacancies.

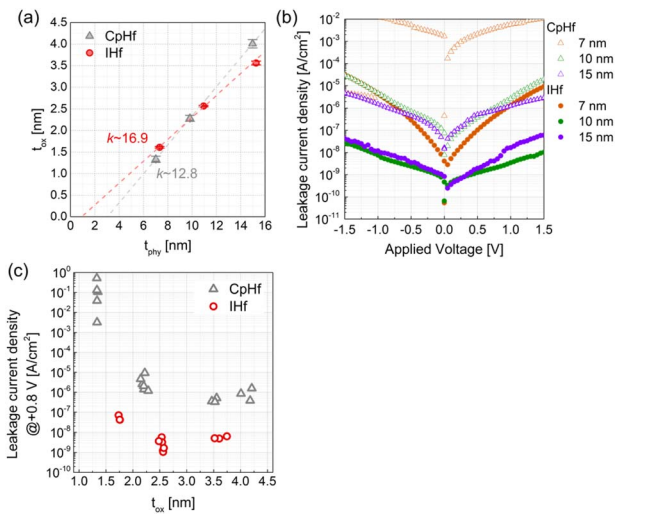

Fig. 4 (a) t_{phy}–t_{ox} plot, (b) J–V curves, and (c) J–t_{ox} plot of HfO_2 thin films varied thicknesses using CpHf and IHf precursors.

This indicates that the suppression of interfacial layer formation when using IHf as a precursor effectively inhibits the formation of oxygen vacancies within the HfO_2 films, contributing to significant improvements in leakage current. These enhancements in the dielectric constant and leakage current characteristics of HfO_2 films deposited with IHf are clearly evident in the leakage current *versus* equivalent oxide thickness (J–t_{ox}) plot (Fig. 4(c)). HfO_2 films deposited with CpHf exhibit high leakage currents of over 10^{-7} A cm^{-2} at an applied voltage of +0.8 V. In particular, at a thickness of 7 nm, which is the practical utilization thickness of the dielectric layer in DRAM capacitors, a very high leakage current of 10^{-2} A cm^{-2} was observed. Conversely, HfO_2 films deposited with IHf demonstrate leakage currents of 10^{-7} A cm^{-2} even at a thickness of 7 nm, achieving leakage currents at levels suitable for the practical utilization in DRAM at a t_{ox} of 1.75 nm.

Conclusions

In conclusion, this study presents a comprehensive analysis of a novel Hf precursor, IHf, synthesized through a three-step process, introducing iodine to the cyclopentadienyl group to enhance its thermal stability and reactivity. The chemical structure and synthesis process were elucidated, demonstrating successful preparation of IHf for use as an ALD precursor. ALD deposition behavior using IHf exhibited slightly faster deposition rates and higher saturation chemisorption density on TiN surfaces compared to CpHf, indicating its superiority as a precursor for HfO_2 thin film deposition. XRD analysis demonstrated that films deposited with IHf exhibited superior crystallinity, even in the as-deposited state, compared to films deposited with CpHf, which remained amorphous until annealing. XPS analysis further confirmed the ideal stoichiometry and absence of nitrogen impurities in HfO_2 films deposited with IHf, in contrast to films deposited with CpHf, which exhibited nitrogen-induced oxygen deficiency and interfacial layer formation. The enhanced properties of HfO_2 films deposited with IHf translated into improved electrical characteristics in MIM capacitors, including higher dielectric constants and significantly lower leakage currents compared to films deposited with CpHf. These improvements were attributed to the suppression of interfacial layer formation and oxygen vacancies within the HfO_2 films when using IHf as a precursor. Overall, the results demonstrate the efficacy of IHf as a precursor for ALD deposition of HfO_2 films, offering potential advancements in the fabrication of high-performance electronic devices, particularly in DRAM applications. The enhanced thermal stability, reactivity, and film properties of IHf make it a promising candidate for future semiconductor manufacturing processes.

Data availability

The data supporting this article have been included as part of the ESI.† Additional data are available upon request from the authors.

Author contributions

Conceptualization, S. P., Y. C., J. P. and W. J.; methodology, S. P., Y. C., J. P. and W. J.; validation, H. L., J. P. and W. J.; formal analysis, S. P., Y. C., S. P., H. L. and K. L.; investigation, S. P. and S. P.; visualization, S. P., Y. C. and K. L.; writing-original draft, S. P., Y. C., H. L., J. P. and W. J.; writing-review & editing, S. P., Y. C., H. L., J. P. and W. J.; project administration, J. P. and W. J.; funding acquisition, J. P. and W. J.

Conflicts of interest

There are no conflicts to declare.

Acknowledgements

This work was partly supported by the GRRC program of Gyeonggi province [(GRRCKYUNGHEE2023-B02), Development of ultra-fine process materials based on the sub-nanometer class for the next-generation semiconductors].

Notes and references

1 R. D. Clark, *Materials*, 2014, **7**, 2913–2944.
2 H. Wong and H. Iwai, *Microelectron. Eng.*, 2006, **83**, 1867–1904.
3 W. Jeon, *J. Mater. Res.*, 2019, **35**, 775–794.
4 J. Robertson, *Eur. Phys. J.: Appl. Phys.*, 2004, **28**, 265–291.
5 D. Vanderbilt, X. Zhao and D. Ceresoli, *Thin Solid Films*, 2005, **486**, 125–128.
6 J. Kim, B. S. Kim, A. J. Lee, D. H. Han, J. H. Hwang, Y. Kim, K.-C. Song, H. Oh, S. Kim, Y. Park and W. Jeon, *Ceram. Int.*, 2022, **48**, 3236–3242.
7 A. J. Lee, B. S. Kim, J. H. Hwang, Y. Kim, H. Oh, Y. Park and W. Jeon, *Appl. Surf. Sci.*, 2022, **590**, 153082.
8 J.-P. Niemelä, G. Marin and M. Karppinen, *Semicond. Sci. Technol.*, 2017, **32**, 093005.
9 M. Popovici, K. Tomida, J. Swerts, P. Favia, A. Delabie, H. Bender, C. Adelmann, H. Tielens, B. Brijs, B. Kaczer, M. A. Pawlak, M. S. Kim, L. Altimime, S. Van Elshocht and J. A. Kittl, *Phys. Status Solidi A*, 2011, **208**, 1920–1924.
10 W. Lee, W. Jeon, C. H. An, M. J. Chung, H. J. Kim, T. Eom, S. M. George, B. K. Park, J. H. Han, C. G. Kim, T.-M. Chung, S. W. Lee and C. S. Hwang, *Chem. Mater.*, 2015, **27**, 3881–3891.
11 D. Triyoso, R. Liu, D. Roan, M. Ramon, N. Edwards, R. Gregory, D. Werho, J. Kulik, G. Tam, E. Irwin, X.-D. Wang, L. B. La, C. Hobbs, R. Garcia, J. Baker, B. E. White Jr and P. Tobin, *J. Electrochem. Soc.*, 2004, **151**, F220–F227.
12 M. Leskelä and M. Ritala, *Thin Solid Films*, 2002, **409**, 138–147.
13 J. Niinistö, K. Kukli, M. Heikkilä, M. Ritala and M. Leskelä, *Adv. Eng. Mater.*, 2009, **11**, 223–234.
14 T. Blanquart, J. Niinistö, M. Ritala and M. Leskelä, *Chem. Vap. Deposition*, 2014, **20**, 189–208.

15 G. Y. Lee, S. Yeo, S. H. Han, B. K. Park, T. Eom, J. H. Kim, S. H. Kim, H. Kim, S. U. Son and T. M. Chung, *Inorg. Chem.*, 2021, **60**, 17722–17732.
16 K. Kukli, *et al.*, *Thin Solid Films*, 2002, **416**, 72–79.
17 M. Ritala, M. Leskela, L. Niinisto, T. Prohaska, G. Friedbacher and M. Grasserbauer, *Thin Solid Films*, 1994, **250**, 72.
18 J. Aarik, A. Aidla, A. A. Kiisler, T. Uustare and V. Sammelselg, *Thin Solid Films*, 1999, **340**, 110–116.
19 H. B. Park, M. Cho, J. Park, S. W. Lee, C. S. Hwang, J. P. Kim, J. H. Lee, N. I. Lee, H. K. Kang, J. C. Lee and S. J. Oh, *J. Appl. Phys.*, 2003, **94**, 3641–3647.
20 J. Niinistö, M. Mäntymäki, K. Kukli, L. Costelle, E. Puukilainen, M. Ritala and M. Leskelä, *J. Cryst. Growth*, 2010, **312**, 245–249.
21 D. C. Won and S.-W. Rhee, *J. Vac. Sci. Technol., B: Nanotechnol. Microelectron.: Mater., Process., Meas., Phenom.*, 2014, **32**, 03D102.
22 L. Aarik, H. Alles, A. Aidla, T. Kahro, K. Kukli, J. Niinistö, H. Mändar, A. Tamm, R. Rammula, V. Sammelselg and J. Aarik, *Thin Solid Films*, 2014, **565**, 37–44.
23 A. R. Choi, S. Seo, S. Kim, D. Kim, S.-W. Ryu, W.-J. Lee and I.-K. Oh, *Appl. Surf. Sci.*, 2023, **624**, 157104.
24 Y. S. Lee, W. Jeon, Y. C. Cho, M. H. Lee, S. J. Jeong, J. S. Park and S. J. Park, *ACS Nano*, 2016, **10**, 6659–6666.
25 F. Peng, Y. Liu, H. Wang, H. Yu and J. Yang, *Chin. J. Chem. Phys.*, 2010, **23**, 437–441.
26 P. G. Wu, C. H. Ma and K. S. Jian, *Appl. Phys. A: Mater. Sci. Process.*, 2005, **81**, 1411–1417.
27 D. Jaeger and P. Jörg, *J. Electron Spectrosc. Relat. Phenom.*, 2012, **185**, 523–534.
28 S. Oktay, Z. Kahraman, M. Urgen and K. Kazmanli, *Appl. Surf. Sci.*, 2015, **328**, 255–261.
29 J. W. Han, H. S. Jin, Y. J. Kim, J. S. Heo, W. H. Kim, J. H. Ahn, J. H. Kim and T. J. Park, *Nano Lett.*, 2022, **22**, 4589–4595.
30 D. S. Kwon, W. Jeon, D. G. Kim, T. K. Kim, H. Seo, J. Lim and C. S. Hwang, *ACS Appl. Mater. Interfaces*, 2021, **13**, 23915–23927.
31 A. J. Lee, S. Lee, D. H. Han, Y. Kim and W. Jeon, *J. Mater. Chem. C*, 2023, **11**, 6894–6901.
32 J. H. Lee, B. E. Park, D. Thompson, M. Choe, Z. Lee, I. K. Oh, W. H. Kim and H. Kim, *Thin Solid Films*, 2020, **701**, 137950.
33 S. Kang, H. Kwon, Y. J. Pu and J. Park, *Mater. Today Energy*, 2021, **21**, 100706.
34 H. Kwon, S. Kang, S. Park, H. Lee and J. Park, *Dyes Pigm.*, 2023, **209**, 110931.
35 G. Bersuker, J. H. Sim, C. S. Park, C. D. Young, S. V. Nadkarni, R. Choi and B. H. Lee, *IEEE Trans. Device Mater. Reliab.*, 2007, **7**, 138–145.
36 A. Kerber, E. Cartier, L. Pantisano, R. Degraeve, T. Kauerauf, Y. Kim, A. Hou, G. Groeseneken, H. E. Maes and U. Schwalke, *IEEE Electron Device Lett.*, 2003, **24**, 87–89.